Journal of Food Engineering 97 (2010) 393–402

Contents lists available at ScienceDirect

Journal of Food Engineering

journal homepage: www.elsevier.com/locate/jfoodeng

CFD modeling of heat transfer and flow field in a bakery pilot oven

Micael Boulet [a], Bernard Marcos [a,*], Michel Dostie [b], Christine Moresoli [c]

[a] Department of Chemical Engineering, University of Sherbrooke, Sherbrooke (Qc), Canada J1K 2R1
[b] LTE-Hydro-Quebec, 600 av. de la Montagne, Shawinigan (Q_C), Canada G9N 7N5
[c] Department of Chemical Engineering, University of Waterloo, Waterloo (On), Canada N2L 3G1

ARTICLE INFO

Article history:
Received 27 July 2009
Received in revised form 22 September 2009
Accepted 25 October 2009
Available online 28 October 2009

Keywords:
CFD
Simulation
Modeling
Baking
Oven
Heat transfer
Heat flux sensor

ABSTRACT

A bakery pilot oven is modeled using computational fluid dynamics software. This approach relies on integration of an instrument into modeled geometry. The instrument is a heat flux measuring device that can be used in the industrial baking process. All three heat transfer mechanisms are considered and coupled with turbulent flow. Turbulence is taken into account via the *k–ε realizable* model whereas the *surface-to-surface* model simulates the radiation. Additionally, buoyancy forces are introduced by means of a weakly compressible formulation. The model predictions show a good qualitative agreement with the experimental measurements. A quantitative agreement was obtained to some extent. Limitations came from the difficulty to measure the temperature of the radiant surfaces of the oven. Operating conditions used are typical of bakery products and, as expected, radiation was the dominant mode of heat transfer. The integration of the instrument was useful for assessing the model. Since it is designed for industrial use, it may be a valuable tool for future challenges in the field, such as simulation of an industrial scale oven.

1. Introduction

Baking operations are complex processes that involve concurrent transport phenomena, heat and mass transfer and air flow. The heat transfer typically involves the three mechanisms, radiation, conduction and convection that differ according to the type of product and oven chamber design and operation. The major factors associated with the heat distribution in the oven chamber include the air flow, the heat supply, the humidity, the oven load and the baking time. The heat absorption by the product is critical for the product quality and varies significantly during the baking operation. High heat absorption occurs at the beginning when the product is at room temperature and is exposed to the high temperature of the oven. The heat absorbed by the product in the initial phase will initiate a number of mechanisms and will lead to the temperature rise in the product which determines the quality of the finished product. At the later stage of the baking operation, the temperature difference between the product and the oven will become smaller leading to lower heat absorption. The mass transfer phenomena are also significant and involve evaporation, condensation and diffusion. The air flow is complex and can be laminar, turbulent or mixed convection.

The efficient operation of a baking oven and the production of baking products of desired and uniform quality will require a good understanding of the heat transfer mechanisms and the associated heat absorption and temperature evolution of the product. Computational fluid dynamics (CFD) modeling represents an appropriate avenue to solve the complex problems associated with baking oven operation. Actually, CFD is rapidly spreading in food engineering as evidenced by the growth in number of papers with CFD application in this field (Norton and Sun, 2006).

Until the last decade, CFD was hardly used for the simulation of baking ovens, whether continuous or batch. Instead, heat and mass transfer was studied using measurements, empirical correlations, global balances, 1D representation, and generally involved analytical solutions (Saxena et al., 1995; Fahloul et al., 1995; Baik et al., 2000; Gupta, 2001; Broyart and Trystram, 2002; Baik and Marcotte, 2002). An important drawback with such approaches is their limited representation of the actual baking environment and the emphasis on the product surface and its core. CFD modeling does not suffer from these limitations and offers adequate modeling tools for computer simulation models that comprise the oven and the cooking environment and will enable better operation, energy efficiency, and design of industrial ovens. In 2000, Verboven et al. (2000) built a 3D CFD model of a forced convection oven. They reported computer power as an important limitation and pointed out that the wall functions associated with the turbulence models should be considered carefully. Mirade et al. (2004)

* Corresponding author.
E-mail address: bernard.marcos@usherbrooke.ca (B. Marcos).

0260-8774/$ - see front matter © 2009 Elsevier Ltd. All rights reserved.
doi:10.1016/j.jfoodeng.2009.10.034

Nomenclature

A	plate surface area (m^2)
C_1	turbulence model parameter
C_2	turbulence model parameter
$C_{1\varepsilon}$	turbulence model parameter
$C_{3\varepsilon}$	turbulence model parameter
C_p	aluminum specific heat capacity (J/kg K)
C_μ	empirical constant in the turbulence model
E_i	emissive power of surface i (W/m^2)
F	view factor
F_{ij}	fraction of energy leaving surface i incident to j
G_b	generation of turbulence kinetic energy due to buoyancy (J/s m^3)
G_k	generation of turbulence kinetic energy due to the mean velocity gradients (J/s m^3)
J_i	radiosity (W/m^2)
S	modulus of the mean rate-of-strain tensor
T	temperature (K)
T_{air}	air temperature (K)
T_i	turbulence intensity (%)
T_w	wall temperature (K)
U_{ref}	mean flow velocity
e	emissivity
e_i	emissivity of surface i
e_w	wall emissivity
$\vec{g}$	gravitational acceleration (9.80665 m/s^2)
h	convective heat transfer coefficient (W/m^2 K)
k	turbulent kinetic energy (J/kg)
l	turbulence length scale
m	mass of aluminum plate (kg)
p	pressure (Pa)
q	surface heat flux (W/m^2)
t	time (s)
u_i	velocity (m/s)
u_i'	fluctuant velocity (m/s)
x_i	coordinate (m)
$y+$	dimensionless wall distance

Greek symbols

ε	turbulent energy dissipation (J/kg s)
λ	thermal conductivity (W/m K)
μ	dynamic viscosity (Pa s)
μ_t	turbulent viscosity (Pa s)
ν	kinematic viscosity (m^2/s)
ρ	density (kg/m^3)
σ	Stefan–Boltzmann constant ($W/m^2 K^4$)
σ_k	turbulence model parameter
σ_ε	turbulence model parameter

simplified the geometry of a continuous tunnel oven and simulated the temperature and the velocity fields. With a fairly fine grid, their model showed good qualitative agreement with experiments. Although their model was unsophisticated, they recognized in CFD a promising and rising tool. A more complex CFD model of a tunnel oven was developed by Therdthai et al. (2004). In addition to mass, momentum, and energy equation, a moving grid was used to directly simulate the travelling trays, allowing deeper transient analysis. They also were able to use their model and improve the operating conditions of the oven. Modifications of this model was proposed by Wong et al. (2007) where the radiation was simulated via the discrete ordinate (DO) model and considered a 2D geometry for finer and improved grids. The 2D assumption shows some improvements, but also limitations, especially for the prediction of the flow field (inherently 3D). Domestic ovens are not omitted from CFD study, as Mistry et al. (2006) presented a three-dimensional model involving unsteady state, natural convection, and radiation. In particular, they analyze the so-called broil cycle.

The objective of this study was to develop a 3D CFD model for the transient description of the heat transfer in a pilot plant oven with radiation as predominant heat transfer mode and coupled with a mixed convection regime. The model includes an inert industrial temperature monitoring instrument, simulating an inert baking product. The model was validated with experimental transient temperature data recorded by the temperature monitoring instrument. The transient heat flux calculated from the temperature measurements was reported. There is a desire for computer simulation models that also comprise the oven and cooking environment, because of the need for better operation, energy efficiency, and design of industrial ovens. At present, CFD modeling is what researchers rely on for oven simulation.

2. Oven description

2.1. Actual oven

The pilot plant oven investigated in this study was designed to reproduce typical baking conditions of industrial baking tunnel ovens but is limited to one section of a tunnel oven and to a static,

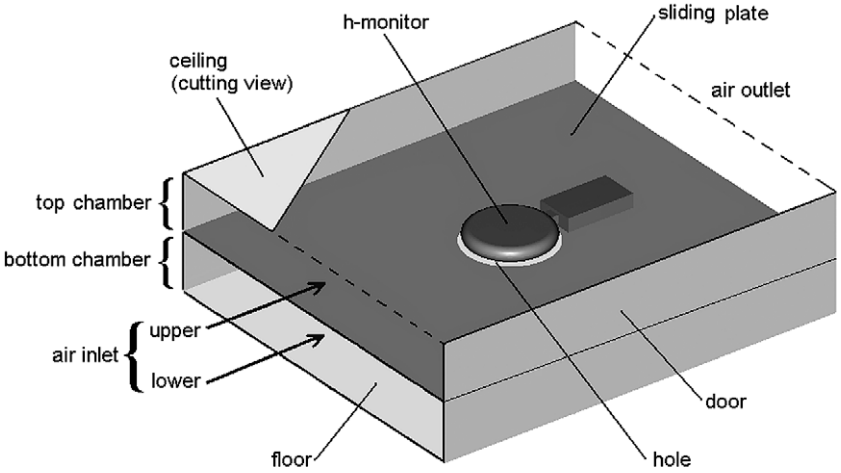

Fig. 1. Geometry of the oven and the h-monitor as used for CFD modeling.

batch type oven. A plate carrying the product is introduced at the beginning of the baking operation and remains in the oven for the entire operation. The plate divides the baking chamber in two equal size chambers (top and bottom) as illustrated in Fig. 1. The dimensions of each chamber are: 1.5 m (width) by 1.4 m (depth) by 0.20 m (height). The bottom chamber does not contain any product, but is used to emulate the bottom zones typically found in an industrial oven, that is, to input heat below the conveyor.

The air is supplied to the oven through a recirculation duct where the air leaving the chamber is conditioned to meet the set point conditions, which can be time dependent. The controlled parameters are: air temperature, air humidity, air velocity, as well as the ceiling and the floor temperature (to induce radiation).

The ceiling and the floor are thin metal sheets exposed to infrared emitters on the side opposite to the baking chamber. The side facing the baking chamber is coated with a black paint of a very high emissivity. Four thermocouples located on each surface (ceiling and floor) are used to control the surface temperature. The positioning of the infrared emitters and the thermocouples is illustrated in Fig. 2.

From the desired operating temperature, the infrared emitters are controlled to maintain a set point temperature at each thermocouple location. These set points differ from the operating temperature. Indeed, previous work focused on heating uniformity in the oven (Zareifard et al., 2006) shows that each thermocouple should have a specific set point in order to reach proper uniform heat flux throughout the chamber. This procedure is automated and the user (the baker) only needs to enter a single operating temperature for ceiling or floor. Operating temperatures for ceiling and floor can be independent of each other but time dependent. It should be pointed out that this operating temperature is used in the model instead of actual thermocouple measurements. Details on how the operating temperatures are related to the thermocouple measurement can be found in Zareifard et al., 2006.

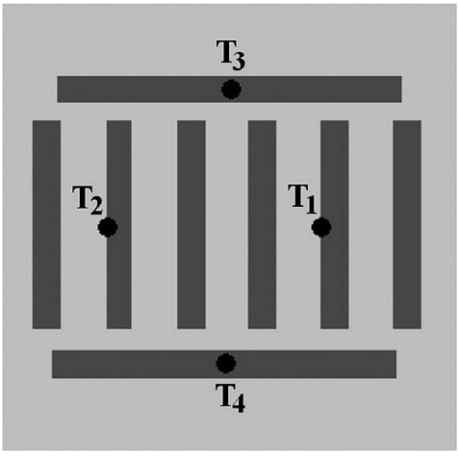

Fig. 2. Schematic top view of ceiling (or floor): Configuration of the heating elements (rectangles) and approximate position of the four thermocouples (●). The diagram is not to scale.

2.2. Temperature monitoring instrument

The monitoring instrument was an h-monitor (Enersyst Development Center Inc. – now owned by TurboChef Technologies). This instrument integrates two thermal targets and a data logger to form a single unit. It is robust and can pass through an industrial oven all together with baking food, revealing useful temperature and heat flux information. The thermal targets are anodized aluminum plates (0.64 cm thickness and 18 cm diameter) embedded in an insulating material such that only the exposed face receives the heat flux. The h-monitor is depicted in Fig. 3 (schematized and pictured).

The h-monitor directly measures the temperature of the two anodized aluminum plates using type-K thermocouples. Transient temperature profiles of the aluminum plates are retrieved from the data logger at the end of each experiment and can be used for heat flux calculations. Indeed, the surface heat flux on each plate is calculated using the simple energy balance equation:

$$q = \frac{mC_p}{A}\frac{dT}{dt}, \tag{1}$$

where: M = mass of the aluminum plate; C_p = specific heat capacity of the aluminum; A = plate surface area exposed; T = plate temperature.

A uniform temperature is assumed for each plate, which is validated by a low Biot number value ($Bi < 0.01$). The term dT/dt is derived from the polynomial best fit of the experimental data.

2.3. Oven simplification for CFD modeling

For CFD modeling, a simplified geometry was considered, the baking chamber and the h-monitor. The system conditioning the baking environment (recirculation duct, blower, and heater) was not modeled. Instead, it is taken into account by proper boundary conditions. Fig. 1 shows the geometry as used in the model.

It is important to note that there are two air inlets and two air outlets (upper and lower, see Fig. 1). The operating conditions for the inlets can be controlled independently. In the current study, the air temperature of the upper inlet differed from the lower inlet.

The ceiling and the floor of the chamber are considered to be smooth surfaces for which the temperatures are imposed. The side walls (including the door) are considered to be uniform thin steel plates. The sliding plate is also assumed as a uniform thin steel plate. The circular hole in the sliding plate under the h-monitor

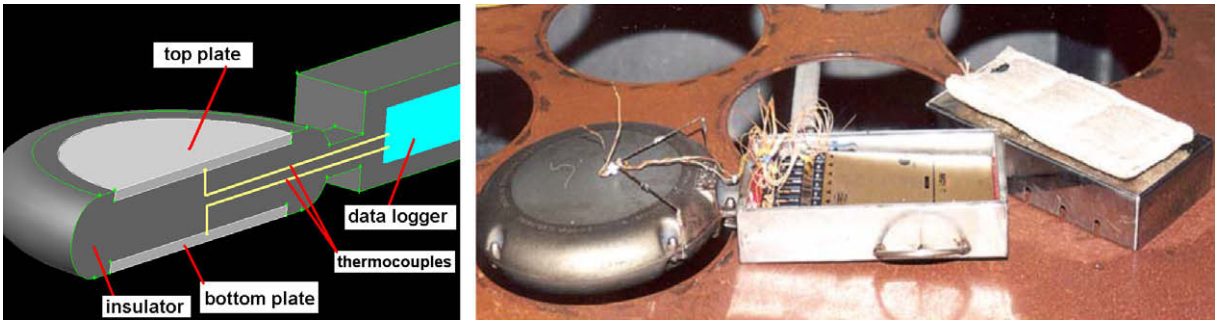

Fig. 3. Left: cross-section of the h-monitor. Right: picture of the h-monitor.

is considered in the geometry. This hole exposes the bottom aluminum plate of the h-monitor to the radiating floor of the oven bottom chamber. The h-monitor is drawn in its integrity, though the data logger and insulator embedding the aluminum plates are considered as a single volume.

3. CFD model

The CFD modeling was developed using FLUENT version 6.3.26.

3.1. Mathematical modeling

The moisture is not considered in this analysis. As a consequence, the air is considered dry. The air flow in the oven chamber is turbulent, as confirmed by the estimation of the Reynolds number (*Re*). The *Re* for an air inlet velocity ranging from 0.5–3 m/s (min–max velocity of the oven) is 4800–29,000.

There are many turbulence models among which to choose, but those available in the software at hand shorten the list. Since averaged values are acceptable for our case, the RANS-based modeling approach is used with the *realizable* k–ε model. The standard k–ε model is a widely used and validated turbulence model (Versteeg and Malalasekera, 1995), but with limitations. Indeed, it is not recommended for cases with flow impinging on surfaces, since the turbulence energy may be over-predicted at the stagnation point (Durbin, 1996). A solution to this is the *realizable* model. The complex geometry of the h-monitor suggests complex flow with stagnation point and thus the *realizable* model was selected.

The continuity and momentum equations written in the RANS format are (in summation convention):

$$\frac{\partial \rho}{\partial t} + \frac{\partial}{\partial x_i}(\rho u_i) = 0 \tag{2}$$

$$\frac{\partial}{\partial t}(\rho u_i) + \frac{\partial}{\partial x_i}(\rho u_i u_j) = -\frac{\partial p}{\partial x_i} + \frac{\partial}{\partial x_j}\left[\mu\left(\frac{\partial u_i}{\partial x_j} + \frac{\partial u_j}{\partial x_j} - \frac{2}{3}\delta_{ij}\frac{\partial u_l}{\partial x_l}\right)\right] + \rho\vec{g} + \frac{\partial}{\partial x_j}(-\rho\overline{u_i' u_j'}) \tag{3}$$

Buoyancy forces are considered by using a weakly compressible formulation. In the weakly compressible formulation, the density depends on temperature, but not on pressure. The Ideal gas law with constant pressure (1 atm) was used to define density.

The last term of Eq. (3) represents the turbulent stress that requires additional closure equation(s) to be solved. Various turbulent models are proposed for the closure equations. Among the turbulent models, the standard k–ε model is an industrial standard (Norton and Sun, 2006). The turbulence is described with two additional variables k (turbulent kinetic energy) and ε (turbulent dissipation) that enables the computation of the turbulent stress and the turbulent viscosity. The *realizable* k–ε model is an improvement of the standard k–ε and consists of the following two transport equations:

$$\frac{\partial}{\partial t}(\rho k) + \frac{\partial}{\partial x_j}(\rho k u_j) = \frac{\partial}{\partial x_j}\left[\left(\mu + \frac{\mu_t}{\sigma_k}\right)\frac{\partial k}{\partial x_j}\right] + G_k + G_b - \rho\varepsilon \tag{4}$$

$$\frac{\partial}{\partial t}(\rho \varepsilon) + \frac{\partial}{\partial x_j}(\rho \varepsilon u_j) = \frac{\partial}{\partial x_j}\left[\left(\mu + \frac{\mu_t}{\sigma_\varepsilon}\right)\frac{\partial \varepsilon}{\partial x_j}\right] + \rho C_1 S\varepsilon - \rho C_2 \frac{\varepsilon^2}{k + \sqrt{\upsilon\varepsilon}} + C_{1\varepsilon}\frac{\varepsilon}{k}C_{3\varepsilon}G_b \tag{5}$$

For Eq. (4), the terms G_k and G_b represent the turbulence energy production by means of the velocity gradient and the buoyancy effect. The negative term represents the energy dissipation. For Eq. (5), the first production term (the second term on the right-hand side of Eq. (5)) is related to the spectral energy transfer (and does not contain the term G_k). The turbulent viscosity μ_t is obtained from the turbulent energy k and the dissipation ε. The terms σ_k, σ_ε, C_1, C_2, $C_{1\varepsilon}$, $C_{3\varepsilon}$ are model parameters. More details about the realizable k-epsilon can be found in Shih et al. (1995) and in FLUENT User's Guide (2006).

In addition to the flow field, the energy equation is considered:

$$\frac{\partial}{\partial t}(\rho C_p T) + \frac{\partial}{\partial x_i}(u_i \rho C_p T) = \frac{\partial}{\partial x_j}\left(\lambda\frac{\partial T}{\partial x_j}\right) \tag{6}$$

For the fluid region, the thermal conductivity, λ, becomes $(\lambda + \lambda_t)$ where λ_t is the turbulent thermal conductivity. Our model does not include source term.

The radiation is the predominant heat transfer mechanism for industrial tunnel ovens. For this study, the radiation was described using the *surface-to-surface* (S2S) model. It is a simple model that does not account for the contribution of the gaseous media. S2S model is based on radiosity, which is the total radiation given off by a surface. The total radiation consists of the emitted energy by the surface and the reflected energy coming from other surfaces. The S2S equation is:

$$J_i = E_i + (1 - e_i)\sum_j^N F_{ij} J_j, \tag{7}$$

where: J_i = radiosity (energy that is given off by surface i); E_i = emissive power of surface i; F_{ij} = fraction of energy leaving i that is incident on j; e_i = emissivity of surface i.Solving for the radiosity, one has a linear system.

3.2. Boundary conditions and assumptions

Boundaries considered for the simplified geometry fall into one of two categories: flow openings and walls. There are two types of flow openings:

1. velocity inlet;
2. pressure outlet;

and three types of wall:

1. insulated;
2. coupled;
3. temperature.

Table 1 summarizes the boundary conditions. The key boundary conditions are related to the oven geometry in Fig. 4.

3.2.1. Velocity inlet

There are two inlet air flows, one for each section of the baking chamber (top and bottom). The air temperature and its velocity are known from experimental measurements. The air velocity is constant while the air temperature is time dependent.

The presence of a grid at the entrance of the oven chamber means that the turbulence properties at the inlet are unknown. The turbulence properties, to be discussed later in this paper, show that their choice has a negligible effect on the h-monitor measurements which supports the choice of the properties presented in Table 1 for a developed flow.

3.2.2. Pressure outlet

The outlet air flow is set as "outlet pressure". A pressure of 1 atm is assumed at outlet. For pressure outlet condition, the CFD software extrapolates all other conditions from the interior of the domain.

Table 1
Boundary conditions.

Modeled equation	Inlet	Outlet	Walls (ceiling, floor)	Walls (h-monitor)	Walls (side walls, sliding plate)
Energy	$T = T_{inlet}(t)$ (T_{inlet} from measurements)	(extrapolates from the interior of the domain)	$T = T_{wall}(t)$ (T_{wall} related to measurements on walls)	Coupled ($q_{fluid} = q_{solid}$)	Coupled ($q_{fluid} = q_{solid}$)
Radiation	$e = 0.95$	$e = 0.95$	$e = 0.95$	$e = 0.90$	$e = 0.40$
Momentum	$v = 0.5$ m/s normal to boundary	$P = 1$ atm	No-slip	No-slip	No-slip
Turbulence	$k = 0.005$ $\varepsilon = 0.0025$	Extrapolates from the interior of the domain	Wall functions	Wall functions	Wall functions

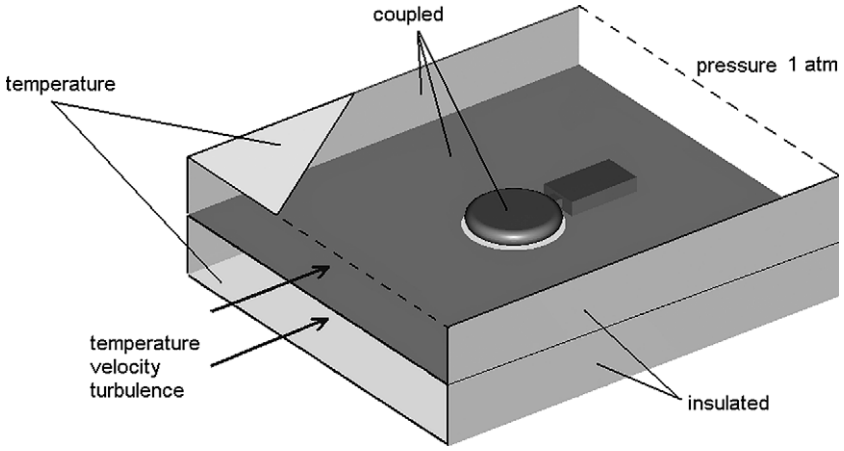

Fig. 4. Major boundary conditions.

3.2.3. Walls

The walls represent most of the boundaries of the system under investigation. The walls are assumed to be insulated, and either coupled or with set temperatures as will be detailed in this section.

All the walls exposed to the outside are assumed to be insulated. This is a good assumption since the baking chamber is wrapped with insulating material.

Only two surfaces have set temperatures: the ceiling and the floor. The ceiling and the floor are thin metal sheets exposed to infrared emitters on the side opposite to the baking chamber. Their set temperature represents an average temperature calculated from the measurements of four individual thermocouples located on each surface as illustrated in Fig. 2. It should be pointed out that the actual temperature of the ceiling and the floor are not uniform because of the configuration of the heating sources. But for ease of simulation, these two boundaries were assumed to be uniform temperature estimated using the control algorithm previously developed by Zareifard et al. (2006).

The walls that separate the fluid and the solid zones (two-sided walls) constitute boundaries that are coupled since there is heat transfer occurring between the fluid and the solid zones. In that case, heat flux each side of the wall is coupled: $q_{fluid} = q_{solid}$.

3.2.4. Initial conditions

Prior to an experiment, the sliding plate and the h-monitor are outside the oven and at room temperature. Meanwhile, the oven is at steady state. The experiment begins by introducing the sliding plate and the instrument in the oven and the oven is switched to transient operating conditions. In order to simulate this, the initial condition in the model is the oven operation at steady state with the sliding plate and the h-monitor set at room temperature.

3.3. Grid

The grid was generated with GAMBIT version 2.3.16, which is mesh generation software for the FLUENT solver. It is a hybrid grid made out of hexahedral, pyramidal and tetrahedral cells. Pyramids are appropriate for zones where the size of the cells increases while hexahedrons are preferred for quality. The growth rate from the finest region to the coarse one must be kept low to avoid poor quality cells that impair the accuracy and convergence. Enforcing this restriction tends to increase the grid size. Because of the complex geometry of the monitoring instrument and the hole, it was not an easy task to reach a good quality grid of reasonable size. The grid size was 2,580,000 cells.

Good CFD practices involve a grid convergence study. However, the wall functions approach is a particular case where grid convergence study fails. Actually, the wall functions dictate the size of the cells near a wall. The mesh requirements are expressed in terms of $y+$, the dimensionless wall distance. With standard wall functions, each wall-adjacent cell's centroid should be located within the so-called log-law layer, $30 < y+ < 300$, but preferably close to the lower bound ($y+ \approx 30$). For a finer grid, FLUENT provides a special near-wall treatment option called "Enhanced Wall Treatment". It is a function that blends linear (laminar) and logarithmic (turbulent) laws-of-the-wall. This helps to resolve the flow down to the viscous layer and required $y+ < 5$. Details about the near-wall treatment as implemented in FLUENT can be found in the FLUENT user's guide (Fluent Inc., 2006).

Since good accuracy is desired for the heat transfer on the top and bottom plate of the h-monitor, the enhanced wall treatment option was employed and the grid at those zones was fine with $y+ \approx 2$. This special treatment was found to be necessary for flow around objects for which the standard wall functions ($y+ > 30$) fail to properly calculate heat transfer as previously pointed out by Verboven et al. (2000).

4. Results and discussion

4.1. Transient temperature and flux profile of the monitoring instrument

The simulations of the transient temperature profile of the top and bottom plate of the h-monitor were achieved according to the methodology presented in Fig. 5. The simulation was carried out in two steps due to the complexity of the numerical problem to solve. The first step consisted of a steady state solution that was obtained by setting all the boundary conditions to the initial conditions. Once the steady state solution was achieved, some boundary conditions were set to their transient values (Table 2). The transient problem was then solved in order to obtain the transient profiles of the temperature and heat flux of the h-monitor.

The temperature predictions show good agreement with the experimental temperature measurement only for the top plate of the instrument (Fig. 6a and b). Indeed, the simulated temperature of the bottom plate is well above the experimental measurements. As the temperature of the bottom plate of the instrument is mainly influenced by the radiation emitted by the floor of the baking chamber, one can suspect that the over prediction of the temperature for the bottom plate of the instrument could be related to an over-estimation of the temperature of the floor of the baking chamber.

The predicted temperature profiles were used to estimate the total heat flux and the contribution of the radiation to the total heat flux as reported in Fig. 7. As expected for this type of oven operation, most of the heat flux is from radiation. For the top plate, about 80% of the heat flux comes from radiation and remains relatively constant during the baking process with the exception of the late stage. The predominance of the radiation was also reported by Broyart and Trystram (2002) for this type of operating condition. At the late stage of baking, the radiation contribution exhibits a characteristic pattern (sudden decrease). This is related to the sudden increase of the upper inlet air temperature. For the bottom plate, the contribution of the simulated radiation heat flux is even more significant, 85% at the beginning and increases to near 99% at the end of the baking process. This can be explained by comparing the temperature of the bottom plate of the instrument and the surrounding air temperature which would be very close. Using Eq. (1), the total experimental heat flux was estimated from experimental temperature data and reported in Fig. 8a and b together with the

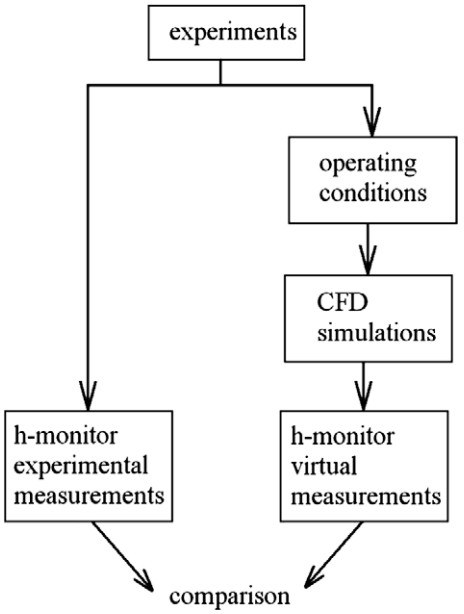

Fig. 5. CFD model development and experimental validation.

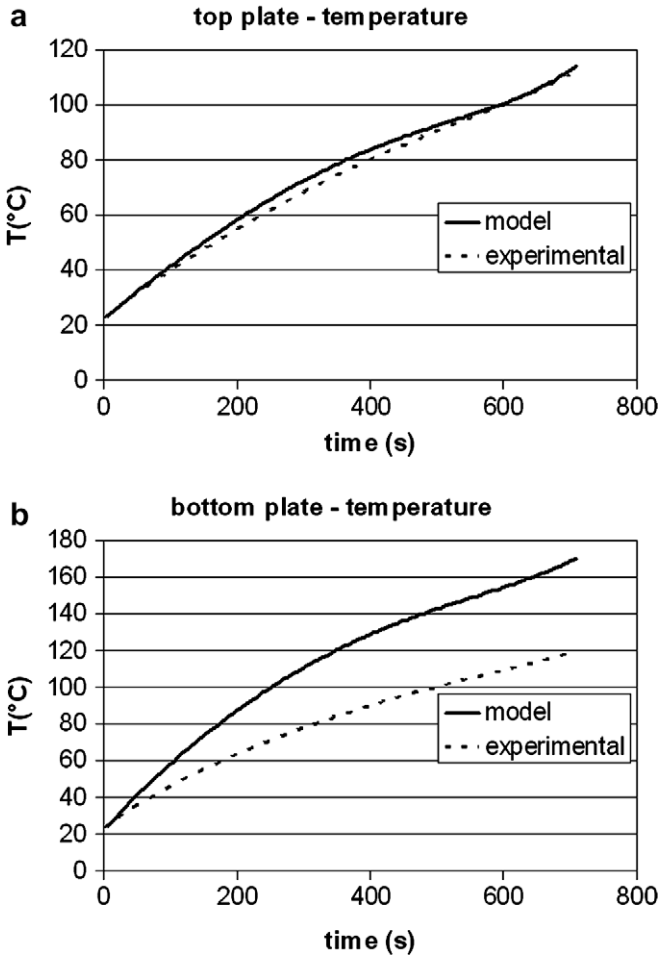

Fig. 6. Model prediction and experimental temperature of the h-monitor: (a) top plate; (b) bottom plate.

Table 2
Initial and transient conditions of time dependant boundaries.

Parameter	Initial value	Transient value
Inlet air temperature	Upper inlet: 150 °C, lower inlet: 185 °C	Upper inlet: temperature, time dependent (min: 150 °C, max: 190 °C) lower inlet: temperature, time dependent (min: 185 °C, max: 190 °C)
Ceiling temperature	223 °C	Temperature, time dependent (min: 173 °C, max: 237 °C)
Floor temperature	317 °C	Temperature, time dependent (min: 242 °C, max: 317 °C)
h-Monitor temperature	22 °C	Coupled wall
Sliding table temperature	22 °C	Coupled wall
Air flow	Steady state solution	Unsteady

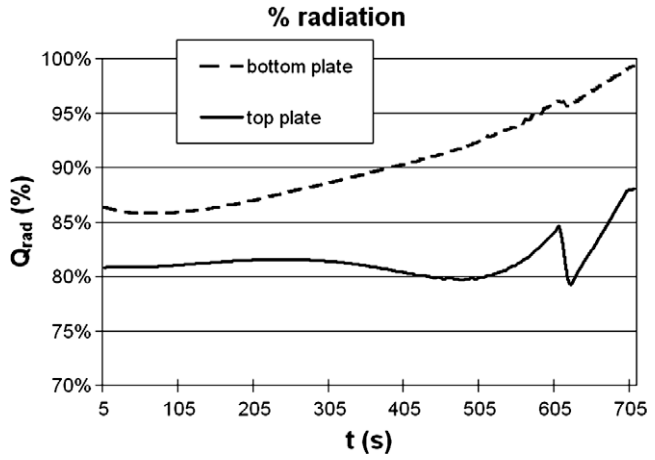

Fig. 7. Contribution of the radiation heat flux for the h-monitor.

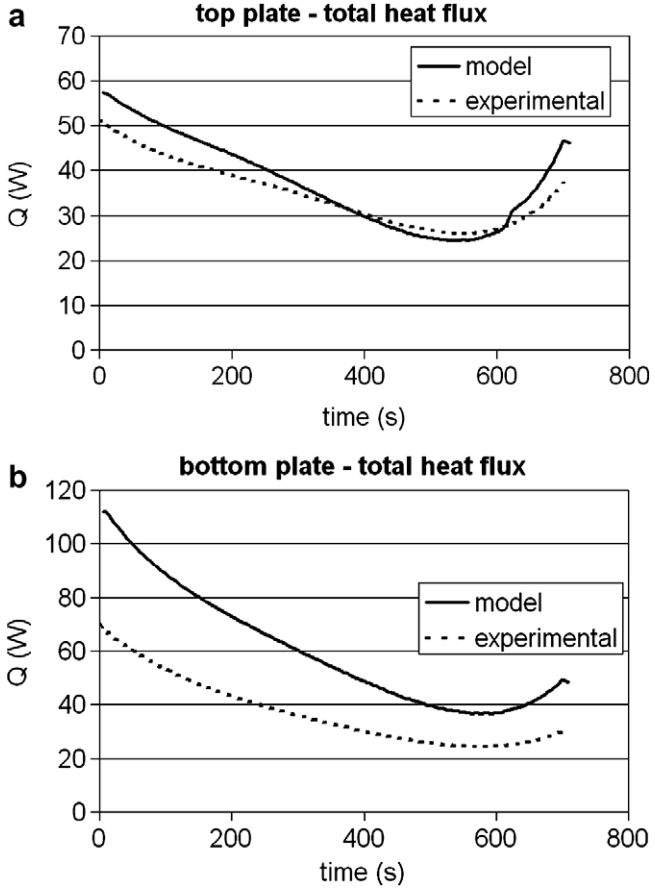

Fig. 8. Total heat flux on top and bottom plates of h-monitor; measured vs. modeled: (a) top plate; (b) bottom plate.

simulated total heat flux. This confirms the over prediction of the heat flux on the bottom plate presented in Fig. 8b.

These results highlight a limitation with the uniform temperature hypothesis. Actually, it is known that the arrangement of the emitters will lead to an uneven floor and ceiling temperature distribution. The operating temperature of the ceiling and the floor of the pilot oven as used in this model is more likely to be representative of the hottest regions of the oven. It is believed that this is more significant for the floor where the quantitative agreement between the model and the experimental data is not good. Also, the operating temperature of the floor was significantly higher than the ceiling during experiment, causing a higher difference between the model and the experimental data. This brings out the difficulty to characterize the temperature for walls with significant radiation.

4.2. Heat transfer contribution of the ceiling and the floor temperatures of the chamber

The temperature of the ceiling and the floor of the chamber dictate the radiation heat transfer, the predominant heat transfer mechanism in this type of baking oven. The estimation of the temperatures of the chamber becomes critical and will play a major role in the heat flux received by the baking product or its equivalent monitoring instrument for this study and the resulting temperature. This being said, their role can be investigated indirectly by analyzing the experimental temperature profile of the monitoring instrument. This analysis should indicate what were the floor and the ceiling temperature that lead to the observed temperature of the monitoring instrument. For this, we make use of a global energy balance on the h-monitor (Eq. (8)), the combination of the total heat flux given by the sum of the radiation heat flux and the convective heat flux.

$$q = \sigma F(e_w T_w^4 - eT^4) + h(T_{air} - T) \tag{8}$$

Eq. (8) can be rearranged in order to give the wall temperature in terms of known information:

$$T_w = \left[\frac{q - h(T_{air} - T)}{\sigma F e_w} + eT^4\right]^{\frac{1}{4}} \tag{9}$$

The convective coefficient, h, is the averaged value obtained from the CFD solution for the base case while T and q are the experimental measurements. The view factor F was obtained with FLUENT via the S2S model. The convective coefficient, h, is approximately 5 W/m^2 °C near the h-monitor. Though the fine and complex grid around the h-monitor involves extensive calculations and is computationally expensive, it allows proper calculation of the convective heat transfer. This may be a solution to the issue of empirical correlations about convective heat transfer coefficient (h), for which generalization is very difficult in complex processes like an oven.

The transient temperature profile for the ceiling and the floor are estimated as T_w in Eq. (9) which is then used as boundary condition in the CFD simulation. The simulated temperature of the h-monitor with this new boundary condition, illustrated in Fig. 9a and b, shows a very good agreement with experimental data for the top and the bottom plate of the h-monitor. When comparing the new T_w estimated from Eq. (9) to the estimates used to develop the predictions for the bottom plate of the monitoring instrument presented previously in Fig. 6b, one realizes that the revised T_w is lower which supports the explanation put forward about the limitations of the uniform wall temperature hypothesis.

4.3. Air flow field

Resolving the air flow field presented numerical difficulties because of the complex geometry and the buoyancy forces. As the sliding plate is initially at room temperature, the bottom part of the baking chamber experiences a mixed regime because the upper boundary is at room temperature while the lower boundary is heated. The inverse scenario occurs in the top chamber where there is a stable stratification. During the late stage of baking, those conditions are less severe with the sliding plate heating up. Hence,

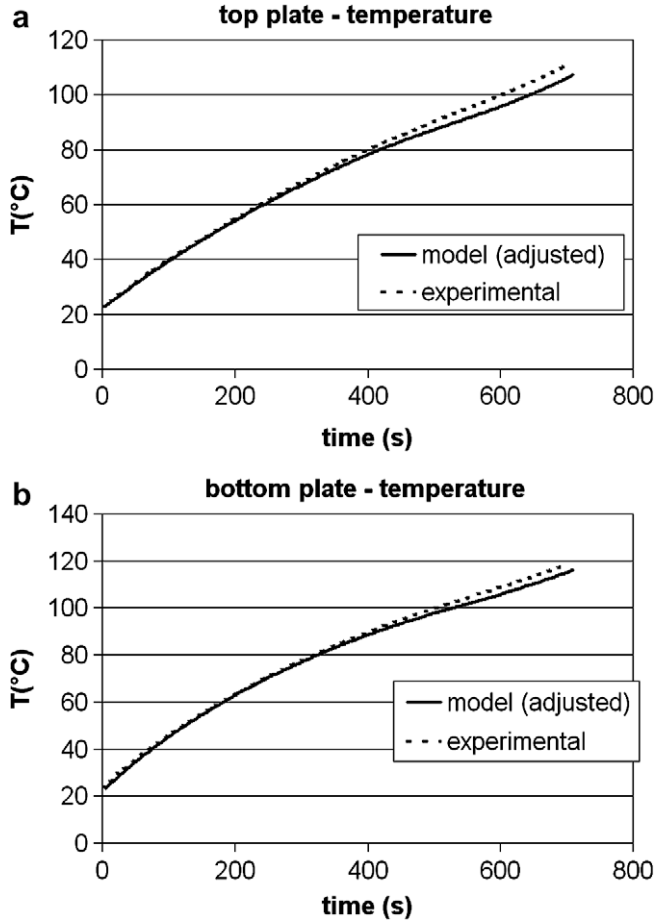

Fig. 9. Temperature of the h-monitor – Model prediction (adjusted ceiling and floor temperature) and experimental measurements: (a) top plate; (b) bottom plate.

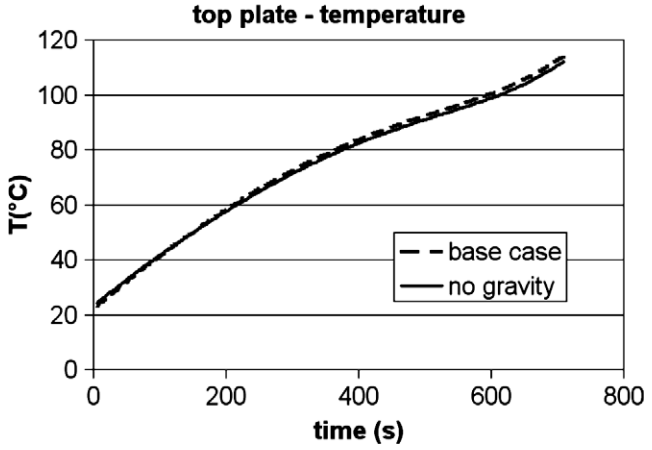

Fig. 10. Temperature predictions of the h-monitor: Effect of the buoyancy forces.

Table 3
Heat transfer on top plate of the h-monitor for different turbulence intensity at the inlet of the chamber.

Turbulence intensity (%)	Convective flux q_c (W)	δ (%)	Total flux q_T (W)	δ (%)
0	10.8	−3%	60.6	−0.6
10	11.2	–	60.9	–
20	11.3	+1%	61.0	+0.2
30	11.3	+1%	61.1	+0.2
40	11.3	+1%	61.0	+0.2
50	11.3	+1%	61.0	+0.1

Table 4
Heat transfer on bottom plate of the h-monitor for different turbulent intensity at inlet.

Turbulence intensity (%)	Convective flux q_c (W)	δ (%)	Total flux q_T (W)	δ (%)
0	14.9	−3%	120.1	−0.4
10	15.4	–	120.6	–
20	15.5	+1%	120.7	+0.1
30	15.6	+1%	120.8	+0.2
40	15.6	+2%	120.8	+0.2
50	15.7	+2%	120.9	+0.3

the beginning of the baking process requires more iteration to achieve convergence.

The buoyancy forces provided a more accurate representation of the flow field. But as buoyancy forces produce a complex flow in the oven, there will be an increase in computational time by a factor of about 10 when compared to neglecting gravity. Since the convective heat transfer represents a small component of the total heat flux, the effect of the buoyancy forces on the temperature profile of the h-monitor was found to be small (Fig. 10). If simulations show that mixed convection exists in the oven, it seems that forced convection is predominant around the h-monitor, regarding heat transfer.

4.4. Role of the turbulence

It is difficult to assess the actual intensity of the turbulence at the inlet of the oven. To overcome this difficulty, we decided to do a parametric analysis on the turbulence intensity and to investigate its effect on the h-monitor heat flux simulated estimates. Taking the opening size of the grid as the turbulence length scale, we can approximate k and ε at inlet from the relationship (Versteeg and Malalasekera, 1995):

$$k = \frac{3}{2}(U_{\text{ref}} T_i)^2 \tag{10}$$

$$\varepsilon = C_\mu^{3/4} \frac{k^{3/2}}{l} \tag{11}$$

U_{ref} is the mean flow velocity through the holes of the grid which is twice the inlet velocity. l is the diameter of those holes (turbulence length scale), T_i the turbulent intensity, and $C_\mu = 0.09$. The turbulence intensity was varied from 0 to 50% with $T_i = 10\%$ taken as reference and using a steady state assumption (Tables 3 and 4). The deviation (δ) from the reference ($T_i = 10\%$) was calculated as follows:

$$\delta = \frac{q - q_{(Ti=10\%)}}{q_{(Ti=10\%)}} \times 100\% \tag{12}$$

Results show that the variation of the turbulence intensity at the inlet of the chamber has negligible effect on the h-monitor heat flux (Tables 3 and 4). Looking at Eq. (10) and Eq. (11), we see that the turbulence dissipation rate, ε, is proportional to k raised to the 3/2 power. Furthermore, the length scale, l, is small (5 mm). Those considerations suggest that for the situation under investigation, where there is a grid at the entrance of the air inlet, the turbulence dissipation should be large. Experimental measurements found in the literature show that turbulence intensity decreases exponentially with the distance from a grid (Kondjoyan and Daudin,

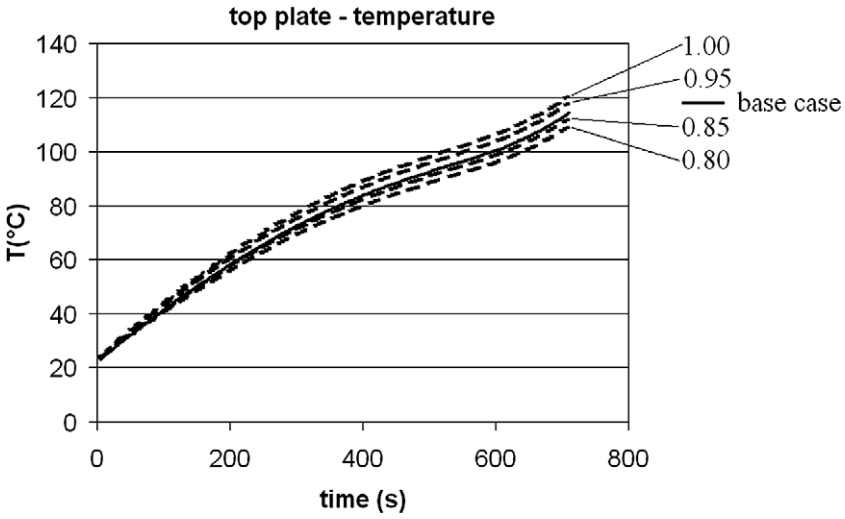

Fig. 11. Temperature predictions of the h-monitor: Effect of the h-monitor emissivity.

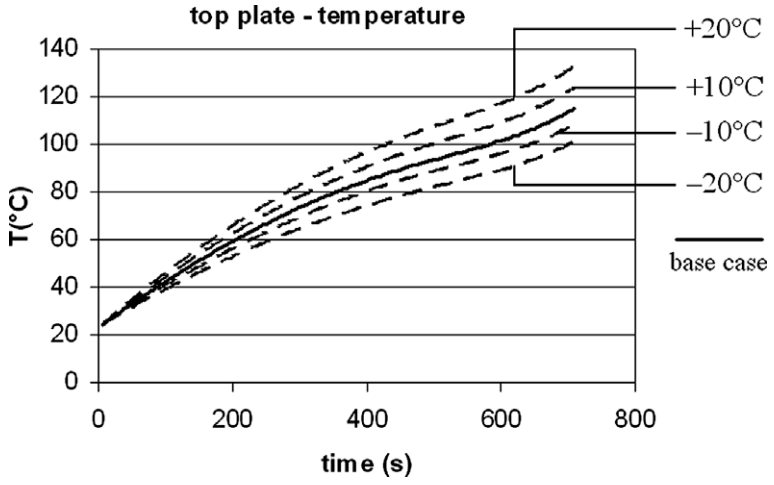

Fig. 12. Temperature predictions of the h-monitor: Effect of the ceiling temperature.

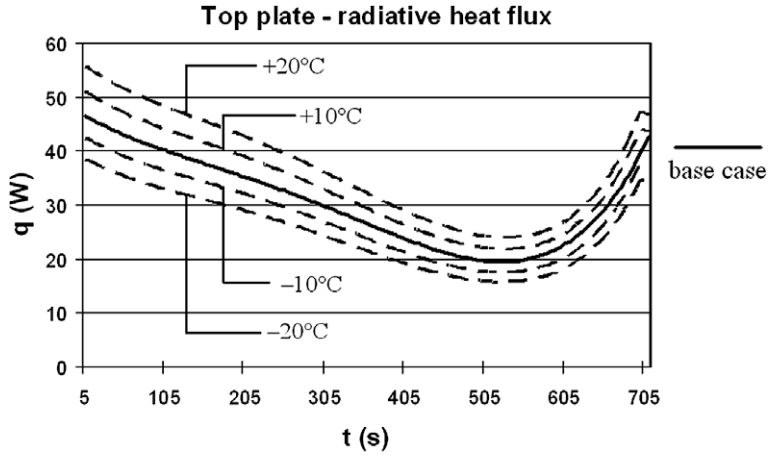

Fig. 13. Heat-flux predictions for the h-monitor: Effect of the ceiling temperature.

1995). This observation explains why the turbulence intensity vanishes before reaching the h-monitor. Hence, for our system the turbulence properties at the inlet have limited influence and it was decided to set k and ε at low values because of faster convergence of the CFD solution.

4.5. Sensitivity analysis

Two parameters, the wall temperature (ceiling and floor) and the emissivity of h-monitor, were selected for the sensitivity analysis. Reducing the air velocity enhances the natural convection and

the flow becomes too complex for convergence with the current mesh. Hence, velocity was not included in the parametric analysis.

The emissivity of the h-monitor is expected to be in the range of 0.9–0.95 (Zareifard et al., 2006). For the sensitivity analysis, the emissivity was set to 0.9 from the base case and then tested from 0.8 to 1. The simulated h-monitor temperature is reported on Fig. 11. For clarity, only the results for the top plate are shown since the effect on the bottom plate is similar. Within the range investigated, the emissivity has little effect.

The wall temperature (T_w) is one of the unknown boundary conditions and is difficult to experimentally estimate accurately (Section 4.2). For the sensitivity analysis, T_w was decreased or increased from −20 to +20 °C around the base case using a 10 °C increment. That is, 4 other cases were tested: −20 °C from base case, −10 °C, +10 °C and +20 °C. The estimates presented in Fig. 12 and Fig. 13, show that T_w has a significant effect on the h-monitor response. An error up to 20 °C on the wall temperature estimate causes an error of approximately 20% for the radiation heat flux and a corresponding error of about 12–18% for the total heat flux. The results of the sensitivity analysis for T_w agree with Eq. (8). The radiation term is predominant with T_w raised to the power of 4 and consequently a small variation of T_w causes a significant variation of the total heat flux.

5. Conclusion

A CFD modeling of the transient heat transfer in a pilot plant baking oven was achieved using an inert temperature monitoring instrument located in the center of the oven as to simulate baking products. The validation of the model temperature predictions was good for the top plate of the monitoring instrument but revealed the difficulty to characterize the temperature for walls with significant radiation.

The surface-to-surface radiation model was adequate in spite of its relative simplicity. The CFD model also shows that radiation is the predominant heat transfer mechanism for an oven with a low inlet air velocity. The importance of the wall temperatures of the chamber was revealed. Not only are those temperatures difficult to determine accurately, but they are sensitive parameters. The resolution of the air flow field was numerically difficult because of the presence of mixed convection. However, it may not be necessary to consider the mixed convection to obtain good estimates of the h-monitor temperature and heat flux profiles.

In conclusion, this study has shown that the coupling of an instrument like the h-monitor with a CFD model is a useful approach for the understanding of the transient behavior of a baking oven and the contribution of the wall temperatures of the chamber. Future work will initially focus on the improvement of the estimation of the temperatures of the walls of the chamber with inverse method approaches. This approach will subsequently be extended to industrial baking ovens where the estimation of the temperature of the walls has long been recognized to be very difficult to estimate accurately which represents a limitation to the energy efficiency operation of industrial ovens.

Acknowledgments

The authors acknowledge professor Nicolas Galanis for his valuable comments during this work. This project was carried out as part of the R&D program of the NSERC Chair in Industrial Energy Efficiency (chair holder: N. Galanis) established in 2006 at Université de Sherbrooke with the support of Hydro-Quebec (Energy Technology Laboratory, LTE), Rio Tinto/Alcan International Ltd., and the CANMET Energy Technology Center (CETC-Varennes, Natural Resources Canada).

References

Baik, O.D., Marcotte, M., 2002. Modeling the moisture diffusivity in a baking cake. Journal of Food Engineering 56, 27–36.
Baik, O.D., Marcotte, M., Castaigne, F., 2000. Cake baking in tunnel type multi-zone industrial ovens Part I. Characterization of baking conditions. Food Research International 33, 599–607.
Broyart, B., Trystram, G., 2002. Modeling heat and mass transfer during the continuous baking of biscuits. Journal of Food Engineering 51, 47–57.
Durbin, P.A., 1996. On the k-3 stagnation point anomaly. International Journal of Heat and Fluid Flow 17, 89–90.
Fahloul, D., Trystram, G., McFarlane, I., Duquenoy, A., 1995. Measurements and predictive heat modeling of heat fluxes in continuous baking ovens. Journal of Food Engineering 26, 469–479.
Fluent Inc., 2006. Fluent user's guide, Version 6.3, Fluent Inc., Lebanon, NH, USA.
Gupta, T.R., 2001. Individual heat transfer modes during contact baking of Indian unleavened flat bread (chapati) in a continuous oven. Journal of Food Engineering 47, 313–319.
Kondjoyan, A., Daudin, J.D., 1995. Effects of free stream turbulence intensity on heat and mass transfers at the surface of a circular cylinder and an elliptical cylinder, axis ratio 4. International Journal of Heat and Mass Transfer 38, 1735–1749.
Mirade, P.S., Daudin, J.D., Ducept, F., Trystram, G., Clément, J., 2004. Characterization and CFD modeling of air temperature and velocity profiles in an industrial biscuit baking tunnel oven. Food Research International 37, 1031–1039.
Mistry, H., Ganapathi-subbu, S., Dey, S., Bishnoi, P., Castillo, J.L., 2006. Modeling of transient natural convection heat transfer in electric ovens. Applied Thermal Engineering 26, 2448–2456.
Norton, T., Sun, D.-W., 2006. Computational fluid dynamics (CFD) – an effective and efficient design and analysis tool for the food industry: a review. Trends in Food Science and Technology 17, 600–620.
Saxena, D.C., Haridas Rao, P., Raghava Rao, K.S.M.S., 1995. Analysis of modes of heat transfer in tandoor oven. Journal of Food Engineering 26, 209–217.
Shih, T.-H., Liou, W.W., Shabbir, A., Yang, Z., Zhu, J., 1995. A New *k*-epsilon eddy-viscosity model for high Reynolds number turbulent flows. Computers Fluids 24 (3), 227–238.
Therdthai, N., Zhou, W., Adamczak, T., 2004. Three-dimensional CFD modeling and simulation of the temperature profiles and airflow patterns during a continuous industrial baking process. Journal of Food Engineering 65, 599–608.
Verboven, P., Scheerlinck, N., Baerdemaeker, J.D., Nicola, B.M., 2000. Computational fluid dynamics modeling and validation of the temperature distribution in a forced convection oven. Journal of Food Engineering 43, 61–73.
Versteeg, H.K., Malalasekera, W., 1995. An Introduction to Computational Fluid Dynamics, The Finite Volume Method.
Wong, S.-Y., Zhou, W., Hua, J., 2007. CFD modeling of an industrial continuous bread-baking process involving U-movement. Journal of Food Engineering 78, 888–896.
Zareifard, M.R., Marcotte, M., Dostie, M., 2006. A method for balancing heat fluxes validated for a newly designed pilot plant oven. Journal of Food Engineering 6, 303–312.